Indonesian Journal of Aerospace Vol. 21 No. 2 December 2023 : pp 109–120 (Moranova et al.)
DOI: 10.55981/ijoa.2023.2669
https://ejournal.brin.go.id/ijoa/

Stress Analysis of Load Cell Adaptor Designs For The Caliber-450mm Solid Rocket Motor Static Test

Starida Moranova[1], Haryadi Abrizal[1], Idris Eko Putro[1], Lilis Maryani[1], Bayu Prianto[1], Azizul Hanif[1], Rika Andiarti[1], Firza Fadlan Ekadj[1], Bagus Wicaksono[1]

[1]Pusat Riset Teknologi Roket, Badan Riset dan Inovasi Nasional, Indonesia
e-mail: staridamaronova@gmail.com

Received: 06-07-2023 Accepted: 28-11-2023 Published: 31-12-2023

Abstract

This study presents a structural analysis of two load cell adaptor designs for a caliber-450 mm solid rocket motor. The structural analysis of a C-shape load cell adaptor and the newly designed truncated-cone shape is presented incorporates a 30-degree truncated disc section and varies the thickness to 30 mm, 25 mm, and 20 mm. The numerical simulation using PATRAN reveals that by altering the arm thickness while maintaining the constant hinge thickness, the 30 mm thickness in the disc section yields the best local maximum stress. However, considering the global maximum stress, the 25 mm thickness emerges as the optimal design. The simulation results show that the 25 mm disc section of the load cell adaptor surpasses the aerospace standard safety factor (SF = 1.5) for both local and global maximum stress.

Keywords: load cell adaptor, stress analysis, solid rocket motor, structural analysis, static test

1. Introduction

The load cell is a sensor that measures thrust in static firing tests for rocket motors. This device operates as a transducer, converts force into an electrical signal, and functions as a force sensor. Load cells and their adaptors exhibit various designs and configurations. One of the load cell types, the S-type load cell is commonly used for research in various fields. In bioengineering, the S-type load cell is used to study muscle fatigue (Moyen-Sylvestre et al., 2022) and hyperkyphosis (Roghani et al., 2018). A study about load cell optimization reviews various types, including S-beam, rectangular beam, shear beam, and pancake beam (Kamble et al., 2020). There are still other types used depending on the utilization like G-type load cell (Chang & Lin, 2013), ring-type load cell (Kamble et al., 2019), and sphere-type.

In the static firing test scenario, a load cell was positioned along with the adaptor responsible for holding the rocket cap while allowing for one degree of freedom. Load cell adaptor also varies in shape. Earlier, NASA's A-1 Test Stand was developed with a cross-shaped frame adaptor to affix an RS-25 engine (Creech et al., 2015). In a previous study by (Abdullah et al., 2012), a load cell consisting of four strain gauges was designed and calibrated to measure rocket thrust through a static test and validate its accuracy. This calibration process utilizes a symmetrical C-shape bending beam. A C-shape load cell adaptor is also used in the amount of a test bench in a study about the design of a solid propellant rocket motor thrust testing system (Fedaravičius et al., 2015).

Historically, load cells for measurement are commonly used in aerospace research and industry. A static thrust test of an unmanned aerial vehicle was assessed to evaluate the propulsion system, utilizing a load cell for force measurement (Khasyofi & Hartono, 2019). Another example involves the design of a 2-axis rocket motor test stand engineered for thrust vectoring, incorporating three load cells suspended via pin joints. Jain et al. (2020) demonstrate

the stress analysis of the stand under specific load conditions by utilizing finite element analysis to assess both the von Mises stress and deformation. Load cells also play a crucial role in the study of the design, optimization, and calibration of wind tunnels. This tunnel was created by assembling six components to form a balanced platform (Khot et al., 2020). This platform incorporated six load cells, each responsible for measuring forces in specific directions. Another study of load cell utilization in aerodynamic wind tunnels focused on configuration optimization (Soni & Priyadarshi, 2013). Research for load cell shape and configuration design for special utilization is commonly conducted (Özbek & Aykaç, 2020), (Ghanvat & Patil, 2012), (Al-Dahiree et al., 2022).

The mechanical strength analysis of a large-scale load cell was conducted using Finite Element Method (Alam, 2015). The focus was on a double-end beam load cell designed for handling heavier loads, such as those found in trucks and tanks. This load cell featured a conventional strain mechanism and Wheatstone circuits. The structural analysis yielded insights into stress and strain simulations. Another application of Finite Element Analysis (FEA) concerning load cells involved a shape optimization of an S-type load cell (Ghanvat & Patil, 2012). Al-Dahiree et al. (2022) use the finite element method to optimize the shape of a load cell. For a larger scale, a large rocket launcher is also analyzed using FEM software as a calculation method (Deng et al., 2017). All the stress analysis studies mentioned earlier employed ANSYS Structural as the primary tool for calculating and simulating structural behavior.

Finite element analysis was utilized to compare structural stress levels between models. Several software packages have been developed to enhance computational processes. While modern, comprehensive, and user-friendly solvers have emerged, traditional solvers like NASTRAN have also been utilized in recent decades. Notably, an underdeveloped rocket test bench underwent analysis using NASTRAN through linear static and dynamic analysis (Fabrino Favato & Magalhães Júnior, 2015). Different FEM software like Pro Engineer software for designing the S-type load cell (Debriand et al., 2018). In their study, the 3D model was halved for enhanced efficiency. The research demonstrated minimal differences between sensitivity values derived from analytical calculations and those obtained from half-model simulations.

During the static test, the applied thrust acted on the load cell adaptor and created a reaction force according to Newton's law. In the preceding static test involving the 450-mm-caliber rocket, a C-shape load cell adaptor was exclusively employed owing to prior failure issues stemming from earlier testing. Therefore, a novel load-cell design was developed to address the occurrence of failure experienced in previous static tests. The suggested new model is created by providing an angle on the disc part (on its arms if viewed from a cross-section), creating a truncated-cone-shape adaptor. This angle is expected to distribute the concentrated pressure. It is considered that if the adaptor arms section to some angles, the forces acting on the moment arms decrease as they are progressively distributed across alternative axes. The angle given is 30 degrees relative to the vertical axis. This truncated-cone model was recently used in a static firing test in the same year in a study of thrust measurement accuracy (Fernandes et al., 2022).

The purposed rocket in this load cell adaptor study has a caliber of 450 mm (Hakiki et al., 2022) and a maximum thrust of 34000 kgf. The purposed rocket in this load cell adaptor study has a caliber of 450 mm (Hakiki et al., 2022) and a maximum thrust of 34000 kgf. In a previous static test, the thrust generated exceeded the calculated prediction, thus in the purpose of studying the adaptor, it will be assumed that the rocket may experience an increase in thrust beyond predictions. A loading of 50000 kgf will be applied to prepare for the worst-case scenario.

The objective of this paper is to explore the new design with various thicknesses under 30 mm, aiming to ascertain the threshold at which the maximum stress approaches the value observed in the initial design. Subsequently, the new design undergoes analysis with three different variations of rod thickness: 30 mm, 25 mm, and 20 mm. By determining the minimum thickness limit based on the maximum stress exhibited by the initial design (C-shape) and identifying the threshold at which maximum stress occurs, the optimal design is derived.

This paper presents a stress analysis of two load cell adaptor configurations, both intended for use with a 450 mm diameter solid rocket cap. The first design features a conventional C-shaped cross-section. In contrast, the second design involves a 30-degree angled disc section from the vertical axis, resulting in an adaptor resembling a truncated cone.

2. Methodology

2.1. Structural Load

A load cell adaptor attached to a test bed in a static test has a load distribution along the circular surface contact to the cap, illustrated in Figure 2-1.

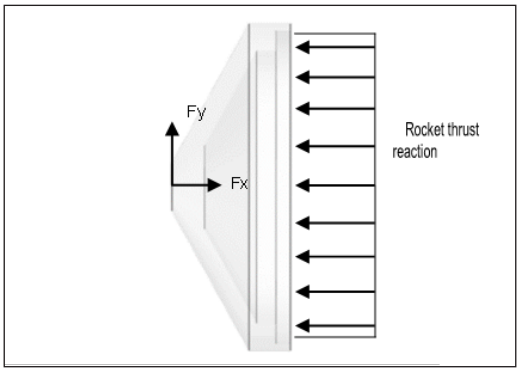

Figure 2- 1: Free body diagram of a load cell adaptor

As the z-axis of the adaptor is fixed (Fz = 0), the deformation will only occur in the x-y plane. To conduct a structural analysis of the component which includes internal stresses, one way to know the failure criteria of a material is by comparing the distortion energy per unit volume of the material between the actual and the yield point refer to Equation (2-1). (Stephens, 2013, Zienkiewicz et al., 2013 and Barsanescu & Comanici, 2017).

$$\frac{1+\mu}{3E}\,\sigma_Y^2 \geq \frac{1+\mu}{3E}(\sigma_1^2 - \sigma_1\sigma_2 + \sigma_2^2) \qquad (2\text{-}1)$$

The term refers to the yield stress and is known as the von Mises stress, which refers to a measure of the stress state of a material. The determination of von Mises stress over finite local points of the adaptor is achieved through the utilization of a numerical method. For modeling and analysis, PATRAN and NASTRAN become the chosen numerical software. Its accuracy was been reviewed in (Fahnline, 2010)) and is widely used in structural analysis for rocket test instruments (Fabrino Favato & Magalhães Júnior, 2015, Setiadi et al., 2022, and Ünal et al., 2018).

2.2. Geometrical Models and Properties

The initial load cell adaptor model geometry is shown in Figure 2- 2:

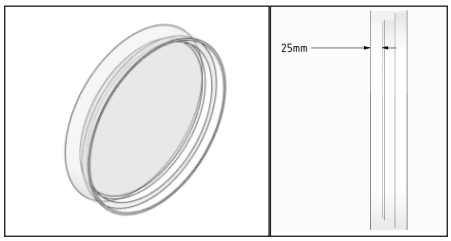

Figure 2- 2: Initial configuration of C-shape load cell adaptor

The new truncated-cone design is angled to 30 degrees and varied with thicknesses of 30 mm, 25 mm, and 20 mm has the geometry as in Figure 2- 3 and Figure 2- 4.

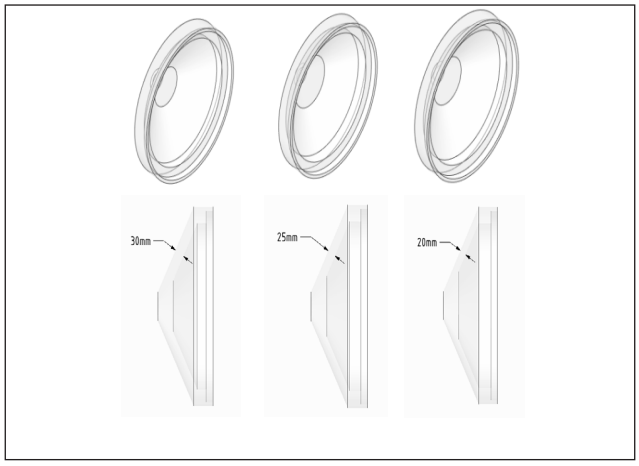

Figure 2- 3: Isometric view of new design load cell adaptor, with thicknesses 30, 25, and 20 mm respectively

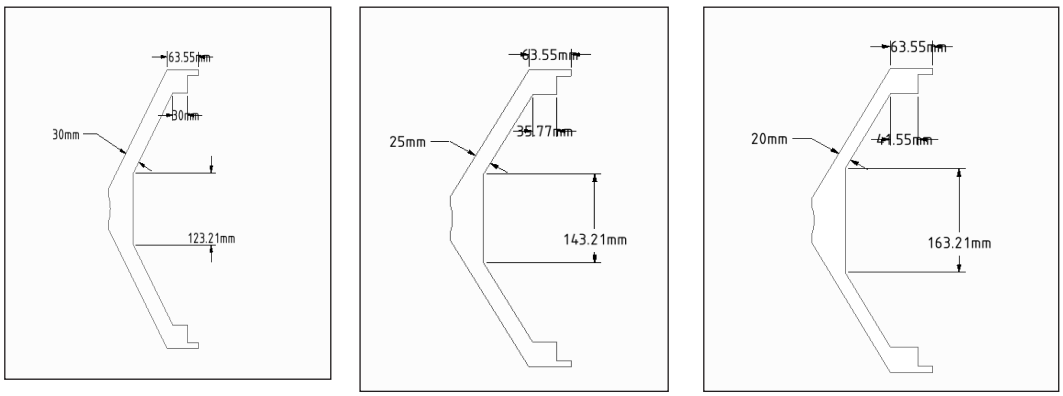

Figure 2- 4: Dimension in cross-section of the model in thickness 30, 25, and 20 mm respectively

Both adaptor models are constructed from S45C material, characterized by the properties in Table 2- 1.

Table 2- 1: Material properties of S45C.

Young's modulus (MPa)	2E5
Poisson's ratio	0.3
Yield Strength (MPa)	343

2.3 Finite Element Analysis and Boundary Conditions

The finite elements were constructed using both isometric and paver methods, resulting in a surface quad mesh. This mesh was subsequently swept to generate uniform solid hex elements. Given that both the adaptor and the rocket motor are aligned along the same axis, it is assumed that the total load is uniformly distributed across the contact surface with the motor. As a result, the simulation omits the utilization of the entire cone to minimize both cost and time.

All models are subjected to an identical total load of 50000 kgf. Since they represent segments of an entire load cell, it's imperative to impose a constraint on the theta angle within cylindrical coordinates. The central points of the adaptor are fixed in place to replicate the conditions of the static test.Top of Form

3. Results and Discussion

The stress analysis by numerical simulation is conducted to determine the stress and deformation along the models. Since the proportion of the models is different owing to the constrained dimension in the mounting area, it is essential to observe locally in the disc section to compare the stress distribution fairly. It is considered crucial since the failure in the prior static test using the C-shape adaptor occurred in the disc section. In this chapter, the stress distribution is presented in the global model and the local disc section. The global stress parameter determines the highest stress and its point in a single model, whereas the local disc stress parameter observes the maximum stress experienced by the disc section.

3.1 Initial C-type Adaptor Model Simulation Result

From the numerical simulation result, the maximum stress and maximum deformation are shown in Table 3-1. Von Mises stress and deformation of the C-shape are shown in Figure 3- 1. In the C-shape adaptor design, the highest value of stress occurs at the hinge connecting the engine mount to the test bed. Taking into consideration the fracture that occurred in the disc region (the stalk segment as shown in Figure 3- 1a), a comparative analysis of the existing stress levels within this disc region is undertaken. In Figure 3- 1a, the maximum stress encountered in the disc region reaches 982 MPa. The greatest stress concentration is observed at the adaptor joint by 2520 MPa as in Figure 3- 1.b., while the stress at the contact surface with the cap measured 357 MPa. Notably, the greatest displacement is localized at the outermost surface of the adaptor, which comes into contact with the surrounding atmosphere and measures 2.93 mm as indicated by Figure 3- 1c.

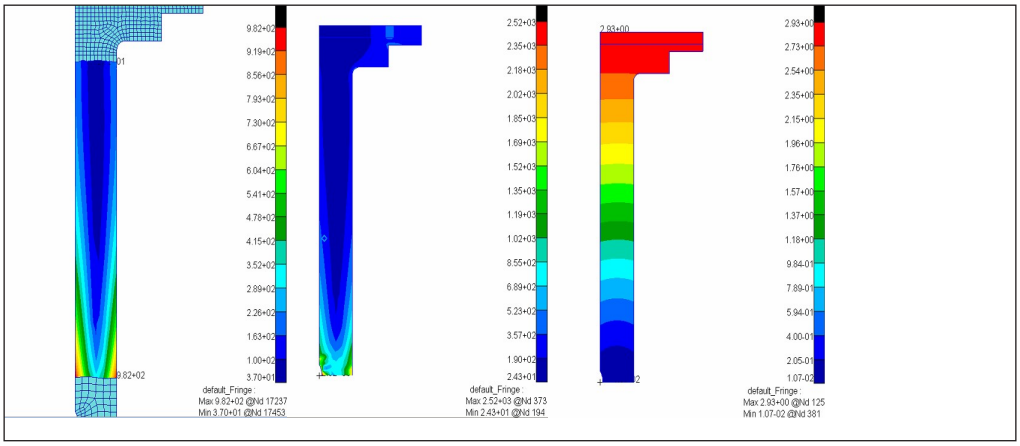

Figure 3-1: (a)Von Mises stress on the local initial model (left), (b) von Mises stress globally on the disc section (middle), (c) deformation

3.2 Maximum Deformation of Truncated-cone Model

The deformation of the truncated-cone models is shown in Figure 3- 2. The maximum deformations in all three thicknesses are located at the top of the adaptor, where the load is applied. The results indicate that the displacement value distribution in thicknesses 25 mm and 20 mm has a larger proportion in the joint and top area. The area below the disc in both models has the minimum displacement value, indicated by the larger dark blue area in Figure 3- 2b and Figure 3- 2c. Meanwhile, in thickness 30, the distribution of displacement value in the joint area is more uniform.

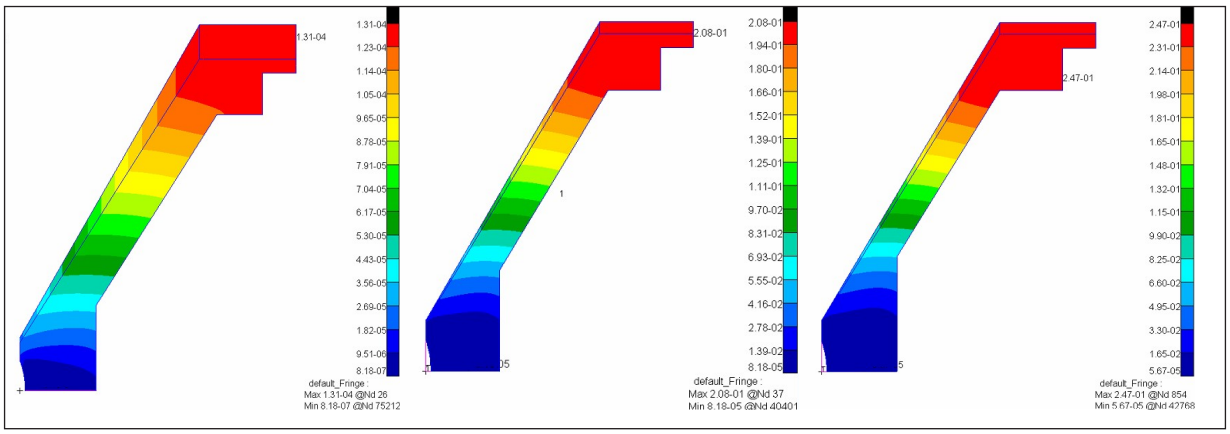

Figure 3-2: Global displacement on the disc section with thicknesses (a) 30 (left), (b) 25 (middle), and (c) 20 mm (right) respectively.

3.3 Local Maximum Von-Mises Stress on Disc Section of The Truncated-cone Model

The local maximum stresses in the disc area of the truncated-cone model by thickness 30, 25, and 20 mm as shown in Figure 3- 3 are 48.6 MPa, 86.9 MPa, and 115 MPa respectively.

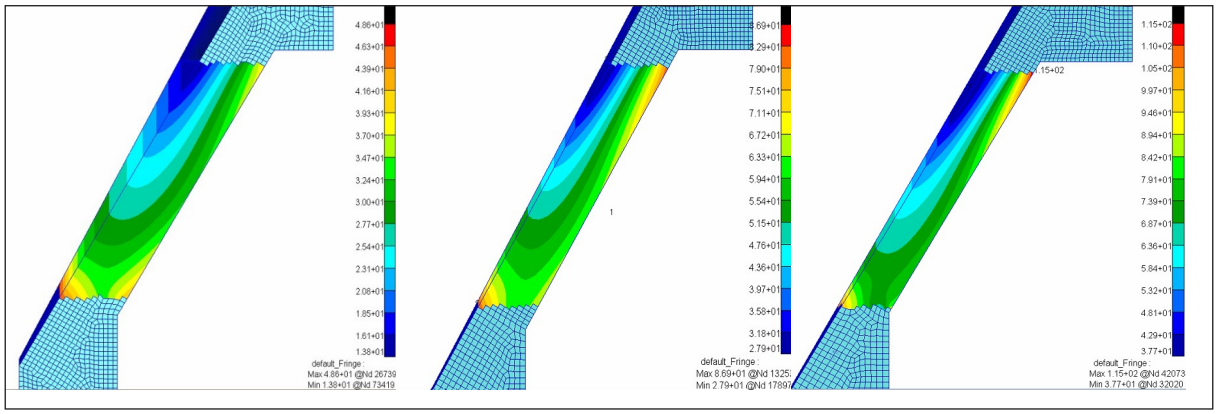

Figure 3-3: Local Von Mises stress on the disc section with thicknesses (a) 30 (left), (b) 25 (middle), and (c) 20 mm (right) respectively.

3.4 Global Von-Mises Stress of The Truncated-cone Model

The global von Mises stress of the truncated model with thickness 30, 25, and 20 are shown in Figure 3-4. The maximum stress occurs at different locations due to stress concentration, with values of 315 MPa, 229 MPa, and 255 MPa for thicknesses of 30, 25, and 20 mm, respectively. The global maximum stress occurs at different points for the three thicknesses and is not directly proportional to the thickness. This discrepancy arises because reducing the disc thickness extends the cap and plug region, consequently altering other geometric dimensions. The maximum stress of 315 MPa is located in the sharp-edged plug area with a thickness of 30 mm. On the other hand, in a cross-sectional comparison of the disc, a thickness of 30 mm yields the lowest value of maximum stress. The maximum stress within the disc region remains reasonably consistent as the thickness increases.

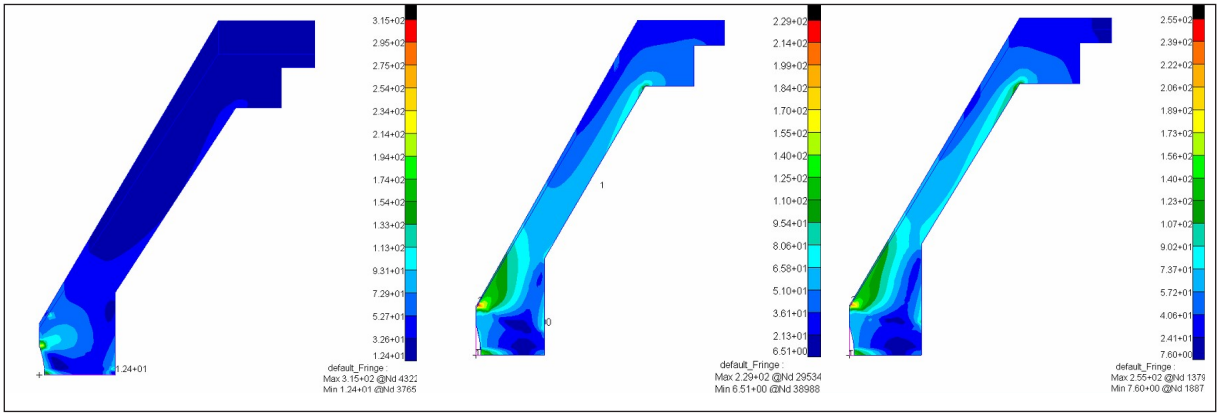

Figure 3-4: Global Von Mises stress in thicknesses (a) 30 (left), (b) 25 (middle), and (c) 20 mm (right) respectively.

3.5 Discussion

The simulation results of the initial C-shape model and the truncated model in thicknesses 30 mm, 25 mm, and 20 mm are summarized in Table 3-1. The calculated safety factor in Table 3-2 is defined as the ratio between the yield strength of material S45C to the maximum working stress from the simulation.

$$SF = \frac{Yield\ Strength}{Maximum\ Working\ Stress} \quad (3\text{- }1)$$

Table 3-1: Maximum local and global stress, and maximum deformation of the configurations.

Model	Maximum Von Mises Stress (MPa)		Maximum deformation (mm)
	Local disc	Global	
C-shape	982	2520	2.93
Truncated-cone shape with a thickness of 30 mm	48.6	315	0.0131
Truncated-cone shape with a thickness of 25 mm	86.9	229	0.208
Truncated-cone shape with a thickness of 20 mm	115	255	0.247

Table 3-2: Safety factor to the yield strength.

Design	SF, based on global maximum stress	SF, based on local disc section maximum stress
C-shape	0.14	0.35
Truncated-cone shape with a thickness of 30 mm	1.09	7.06
Truncated-cone shape with a thickness of 25 mm	1.50	3.95
Truncated-cone shape with a thickness of 20 mm	1.35	2.98

The C-shape adaptor from the prior static test has the SF<1. This happened because the load from the prior tests had a maximum thrust of 34000 kgf where the adaptor experienced a failure. The load used in this study is 50000 kgf to compare the strength uniform loadings to the new truncated-cone design, which has the design requirement to hold a loading of 50000 kgf.

Figure 3- 5: Static test with C-shape adaptor, before and after burning.

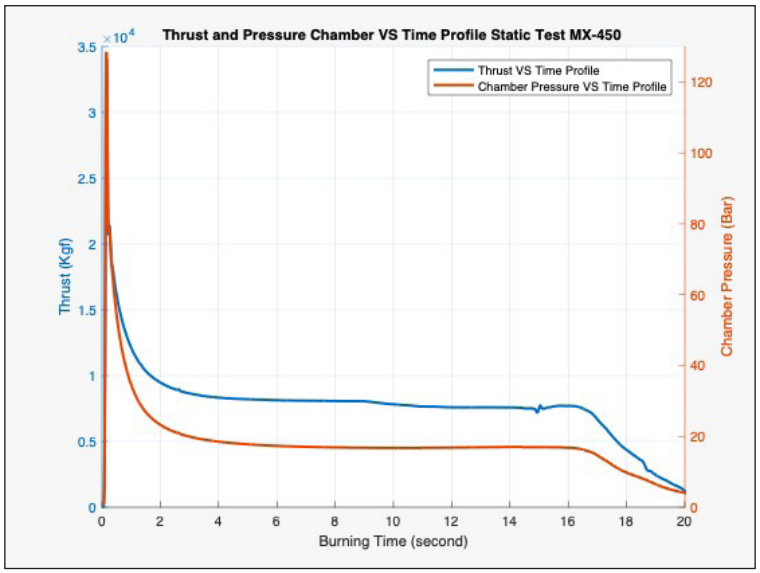

Figure 3- 6: Thrust profile of the static test.

In a prior static test utilizing a C-shape adaptor refer to Figure 3- 1, it is shown after the burning time, the load cell adaptor is compressed as a reaction to the thrust loading. The thrust generated exceeded the calculated prediction and failed to the thrust of 34000 kgf. A new model with a thickness of 30 mm had already been incorporated in a following caliber 450-mm static test. Figure 3- 2 illustrates the side views of the updated design adaptor, highlighting its seamless integration with the rocket motor and its connection to the test bed. Notably, throughout this test, the adaptor demonstrated remarkable resilience, displaying no indications of failure after the static test.

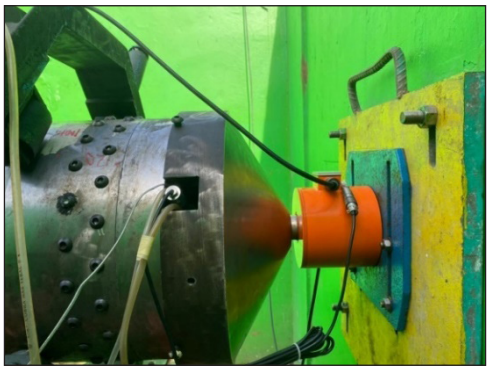

Figure 3- 7: Static Firing Test of the 450-mm-caliber Rocket Motor Using the New Load-Cell Adaptor Design

As in section 3.4, a high-stress concentration in the edged mount occurred in a thickness of 30 mm. Modifying the thickness of the disc section while keeping the mount dimension constant leads to variation in the moments of inertia and the perpendicular distance from the maximum principal stress location to the neutral axis of each geometry. Reducing the disc

thickness results in additional thickness in the mounting section, as seen in Figure 2- 4. This leads to a more evenly distributed stress concentration in the 25 mm and 20 mm thickness configurations due to the increased thickness in the mounting section. The principal stress relation to the inertia is given by Equation (3- 2).

$$\sigma = \frac{My}{I} \tag{3- 2}$$

As M is the moment occurred, y is the distance from the centroid to the maximum stress location, and I is the moment of inertia. The moment of inertia and the centroid location of each cross-section is calculated in Table 3-3.

Table 3-3: Geometrical comparison.

Disc thickness	Hinge thickness (mm)	Moments of Inertia (mm^4)	Centroid distance to the maximum stress location (mm)
30	123.21	5.57E+07	108.42
25	143.21	5.45E+07	105.8
20	163.21	5.34E+07	119

4. Conclusions

The new design of the truncated-cone-shaped load cell adaptor with a thickness of 30 mm withstands the applied load of the rocket thrust, which has been demonstrated by both simulation and experimental static tests. However, the simulation revealed that the disc area exhibits overstrength and exceeds the design requirements and goals in addition to the global maximum stress. Reducing the thickness to 25 mm and 20 mm still does not exceed the yield strength, with safety factors based on global maximum stress being 1.50 and 1.35, respectively.

Optimizing the adaptor thickness to 25mm for the truncated-cone load cell design is considered the best option as the 30mm thickness has the highest stress concentration at the hinge in the global stress distribution. The new design with a thickness of 25 mm can reduce the maximum stress of the original design to 2291 MPa and the maximum deformation to 0.85 mm.

The new design in the analysis is created without a fillet and has sharp edges in some places that affect stress concentration. The maximum stress of all variations did not exceed the material yield. However, if a reduction in maximum stress is desired, rounding may be required.

Acknowledgments

This project is supported by the Government of the Republic of Indonesia through RIIM-LPDP Research Program Batch 1 Year 2022, Grant No. B-808/II.7.5/FR/6/2022 and B-9546/III.1/KS.00.00/6/2022. The authors are also immensely grateful to the National Research and Innovation Agency of Indonesia (BRIN) and the Research Centre for Rocket Technology for supporting this research activity.

References

Abdullah, N. H., Wahida, T. F., Azmin, F., & Ammar, A. (2012). Load cell application in rocket thrust measurement system. *Applied Mechanics and Materials*, *225*, 437–441. https://doi.org/10.4028/www.scientific.net/AMM.225.437

Al-Dahiree, O. S., Tokhi, M. O., Hadi, N. H., Hmoad, N. R., Ghazilla, R. A. R., Yap, H. J., & Albaadani, E. A. (2022). Design and Shape Optimization of Strain Gauge Load Cell for Axial Force Measurement for Test Benches. *Sensors*, *22*(19), 7508. https://doi.org/10.3390/s22197508

Barsanescu, P. D., & Comanici, A. M. (2017). Von Mises Hypothesis Revised. *Acta Mechanica*, *228*(2), 433–446. https://doi.org/10.1007/s00707-016-1706-2

Creech, S. D., Crumbly, C. M., & Robinson, K. (2015). NASA's Space Launch System Mission Capabilities for Exploration. *International Astronautical Congress*. https://doi.org/20150021464

Debriand, R., Doloksaribu, M., & Damanik, I. (2018). Design of Weight Sensor Load Cell Type S. *Metal Journal of Indonesia*, *40*.

Deng, B., Guo, Y., Zhang, A., & Tang, S. (2017). Finite element analysis of large rocket launcher. *Proceedings of the 2017 5th International Conference on Frontiers of Manufacturing Science and Measuring Technology (FMSMT 2017)*. https://doi.org/10.2991/fmsmt-17.2017.223

Fabrino Favato, L., & Magalhães Júnior, P. A. A. (2015). Linear Static and Dynamic Analysis of Rocket Engine Testing Bench Structure using the Finite Element Method. *Journal of Engineering Research and Applications*, *5*(4), 70–77. www.ijera.com

Fahnline, J. B. (2010). An evaluation of residual vectors in the commercial finite-element program NASTRAN. *The Journal of the Acoustical Society of America*, *127*(3_Supplement), 1849–1849. https://doi.org/10.1121/1.3384368

Fedaravičius, A., Račkauskas, S., Survila, A., & Patašienė, L. (2015). Design of The Testing System for Solid Propellant Rocket Motor Thrust Measurements Using Mathematical Modelling Techniques. *Journal of Measurement in Engineering*, 123–131.

Fernandes, F. A. C., Souto, C. d'Andrade, & Pirk, R. (2022). Static Firing Tests of Solid Propellant Rocket Motors: Uncertainty Levels of Thrust Measurements. *Journal of Aerospace Technology and Management*, *14*. https://doi.org/10.1590/jatm.v14.1270

Ghanvat, M. S. M., & Patil, G. (2012). Shape Optimization of "S" Type Load Cell Using Finite Element Method. *International Journal of Engineering Innovation & Research*, *1*(3), 2277–5668.

Hakiki, Duhri, R. A., Putro, I. E., & Hakim, A. N. (2022). Flight Identification Simulation of Performance RX-450. *Journal of Aerospace Technology*, *20*(1), 45–54.

Hilman Syaeful Alam. (2015). Numerical Study of Structural Integrity and Strain Response of Double End Beam Load Cell Using Finite Element Simulation. *2015 International Conference on Automation, Cognitive Science, Optics, Micro Electro-Mechanical System, and Information Technology (ICACOMIT)*, 41–45.

Jain, U., Shukla, H., Kapoor, S., Pandey, A., & Nirwal, H. (2020). Design and analysis of a 2-axis rocket motor stand for thrust vectoring. *AIAA Propulsion and Energy 2020 Forum*, 1–9. https://doi.org/10.2514/6.2020-3920

Khasyofi, M., & Hartono, F. (2019). Development Testing Method and Analysis Static Thrust for Propeller-Based Propulsion. *IOP Conference Series: Materials Science and Engineering*, *645*(1). https://doi.org/10.1088/1757-899X/645/1/012015

Khot, R., Kandagal, S. B., & Sharana Basavaraja, J. (2020). Design, Optimization, and Calibration of 6-Component External Wind Tunnel Balance. *International Journal of Scientific & Engineering Research*, *1*(11). http://www.ijser.org

Özbek, E., & Aykaç, B. (2020). A Load Cell Design that can be utilized for The Testing of Reinforced Concrete Members. *Gazi University Journal of Science*, *7*(4), 106–111. http://dergipark.gov.tr/gujsa

Setiadi, Wicaksono, B., Muzayadah, N. L., Wandono, F. A., & Nurtiasto, T. S. (2022). Investigation on the Mechanical Properties of the Post-Static Fire Testing Effect of Graphite Material used in the RX320 Rocket Motor Nozzle. *Journal of Physics: Conference Series*, *2243*(1), 012050. https://doi.org/10.1088/1742-6596/2243/1/012050

Soni, A., & Priyadarshi, P. (2013). Finite Element Analysis and Optimization of a Beam Type Load Cell for an External Balance Design. *Proceedings of National Conference on Wind Tunnel Testing*.

Stephens, R. C. (2013). *Strain Energy, Theories of Failure* (p. 301). Elsevier.

Ünal, A., Yaman, K., Okur, E., & Adlı, M. A. (2018). Design and Implementation of a Thrust Vector Control (TVC) Test System. *Journal of Polytechnic*, *21*(1), 497–505. https://doi.org/10.2339/politeknik.404009

Zienkiewicz, O. C., Taylor, R. L., & Zhu, J. Z. (2013). *The Finite Element Method: its Basis and Fundamentals* (7th ed., Vol. 1). Elsevier. https://doi.org/10.1016/C2009-0-24909-9